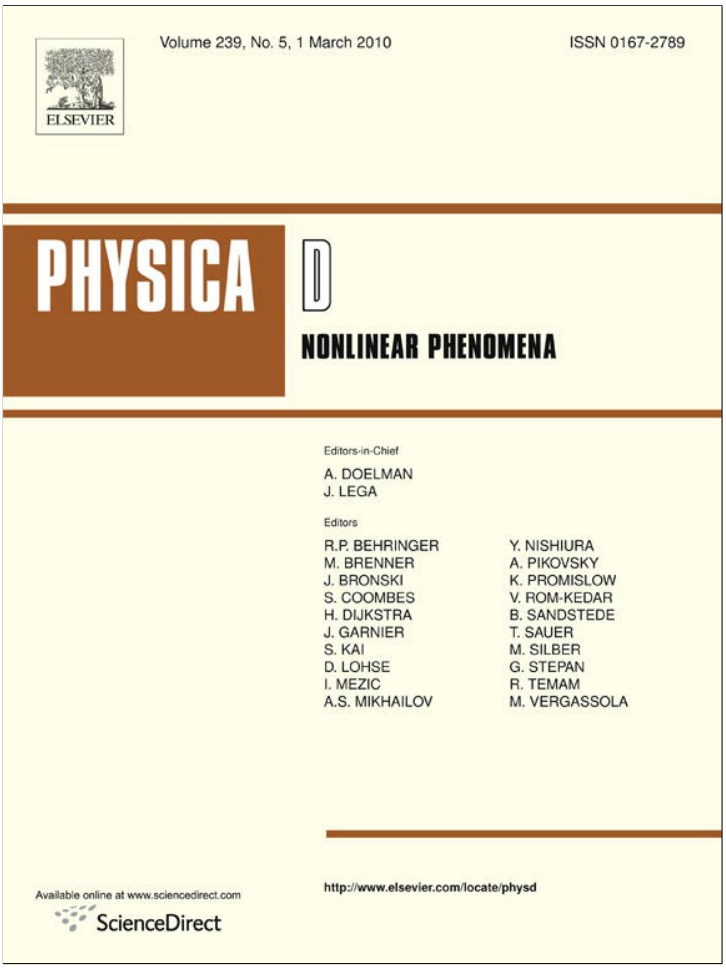

Physica D 239 (2010) 258–268

Contents lists available at ScienceDirect

Physica D

journal homepage: www.elsevier.com/locate/physd

Low-dimensional nonlinearity of ENSO and its impact on predictability

Youmin Tang*, Ziwang Deng

Environmental Science and Engineering, University of Northern British Columbia, Prince George, BC, Canada

ARTICLE INFO

Article history:
Received 29 January 2009
Received in revised form
20 September 2009
Accepted 11 November 2009
Available online 4 December 2009
Communicated by H.A. Dijkstra

Keywords:
EL Nino
Nonlinearity of climate system
Predictability
Bred vector

ABSTRACT

Using a hybrid coupled model, we perform a bred vector (BV) analysis and retrospective ENSO (El Niño and the Southern Oscillation) forecast for the period from 1881 to 2000. The BV local dimension and BV-skewness inherent to the intensity of nonlinearity are analyzed. Emphasis is placed on exploring the nature of the low-dimensional nonlinearity of the ENSO system and the relationship between BV-skewness and model prediction skills. The results show that ENSO is a low-dimensional nonlinear system, and the BV-skewness is a good measure of its predictability at the decadal/interdecadal time scales. As the low-dimensional nonlinearity of ENSO is weakened, high predictability is attained, and vice versa. The low-dimensional nonlinearity of ENSO is also investigated and verified using observations.

Another finding in this study is the relationship between the error growth rate (BV-rate) and actual prediction skill. While there is a good positive correlation between them in some decades, the BV-rate demonstrates a strong inverse correlation with the prediction skill in other decades. The BV-rate components contributed by the nonlinear process play a dominant role in quantifying ENSO predictability. The possible mechanism for the link between BV-rate, BV-skewness and ENSO predictability is discussed.

1. Introduction

A classic framework of predictability study is to analyze the optimal growth of initial errors. The initial patterns exciting the optimal error growth, often called optimal initial modes and used for constructing ensembles, can generate maximum uncertainties in predictions or lowest predictability. One widely used method to analyze the optimal growth of initial errors is the bred vector (BV), first proposed in the 1990s by Toth and Kalnay [1,2]. By construction, the BV is closely related to Lynapunov vectors. While the BV has been widely used in weather forecasts and geophysical fluid dynamics (e.g. [3–6]), it has relatively few applications in climate predictions. Cai et al. [7] first used the breeding method to investigate the ENSO predictability in the ZC model [8]. Yang et al. [9] implemented the breeding method in the NASA Seasonal-to-Interannual Prediction Project (NSIPP) coupled general circulation model.

An important application of the BV technique is to identify the effective dimension of the subspace of BVs, the BV-dimension. The BV-dimension measures locally the dimension of a dynamic system, which is inherent to the complexity of the dynamical system. It was proposed by Patil et al. [4] and has been applied to study the local predictability of some dynamical systems (e.g. [10,5,11,6]); however, the BV-dimension is not effective in measuring the intensity of nonlinearity. To explore the intensity of nonlinearity of the climate system and its impact on predictability is an important issue in climate predictability study.

In this study, we attempt to develop a measure to quantify the intensity of nonlinearity in a dynamical system under a given background (e.g., a prediction run starting from the given initial state). With this new measure and BV-dimension, the low-dimensional nonlinearity of ENSO can be investigated, including its temporal and spatial variations. The other objective of this study is to use the BV to explore ENSO predictability and produce statistically robust results. Towards these goals, the BV is employed in a hybrid coupled model for a long period, from 1881 to 2000. Meanwhile, the retrospective ENSO prediction is performed using the same model for the same period. Emphasis is placed on exploring the nature of low-dimensional nonlinearity of the ENSO system and its impact on model prediction skill. Under the assumption of a perfect model scenario, the model prediction skill represents the potential predictability. Generally, there are two kinds of source that limit ENSO predictability: the chaotic behavior of the nonlinear dynamics of the coupled system (e.g. [12,13]); and the stochastic nature of the coupled system characterized by weather noise and other high-frequency variations, such as westerly wind bursts and Madden–Julian oscillation (e.g. [14–17]). It is still not clear which source plays the dominant role. Thus, the impact of the low-dimensional nonlinearity of ENSO on predictability will provide insights on this central question challenging the ENSO community.

This paper is structured as follows: the model and breeding technique are introduced in Section 2; the resulting BV-dimension and BV-skewness are presented in Section 3; the low-dimensional

* Corresponding author.
E-mail address: ytang@unbc.ca (Y. Tang).

0167-2789/$ – see front matter © 2009 Elsevier B.V. All rights reserved.
doi:10.1016/j.physd.2009.11.006

nonlinearity of ENSO is further verified using real-world observations in Section 4; in Section 5, the relationship between the low-dimensional nonlinearity of ENSO and its predictability is investigated in details; and in Section 6 there is a discussion and a conclusion.

2. Model and BV analysis

2.1. Model

The hybrid coupled model (called HCM) is composed of an oceanic general circulation model (OGCM) coupled to a statistical atmospheric model. The OGCM is the latest version of NEMO (Nucleus for European Modeling of the Ocean), identical to that used in [18]. Details of the OGCM are given at http://www.lodyc.jussieu.fr/NEMO/. The statistical atmospheric model in the HCM, a linear model that predicts the contemporaneous surface wind stress anomalies from sea surface temperature anomalies (SSTAs), was constructed by the singular vector decomposition (SVD) method with a cross-validation scheme. During the initialization of the HCM, the OGCM was forced by the sum of the associated wind anomalies computed from the atmospheric model and the observed monthly mean climatological wind stress.

To perform long-term hindcasts with the HCM, the past wind stress data is required to initialize forecasts. Using historic SST as predictors and the SVD technique, we reconstructed a long-term wind stress dataset from 1881 to 1947 [19]. With the reconstructed winds, the assimilation of SST was performed for the HCM to produce initial conditions of predictions, using the Ensemble Kalman Filter (EnKF) [19]. The retrospective forecasts by the HCM for the period 1881–2000 have been analyzed in detail in [18,20].

2.2. Breeding method

In general, there are two approaches to derive the BV: one-sided and two-sided self-breeding techniques, of which we used the latter in this study. In the two-sided self-breeding algorithm, the BV is obtained by adding two sets of initial random perturbations with opposing signs to the HCM. The two perturbed models are integrated in time, and their difference, scaled by twice the rescaling factor, is the bred vector. The initial perturbations are produced from a normal distribution with a mean of zero and a variance of a specified value that is 10% of the variance of model heat content anomalies of the upper ocean 250 m (HCAs). Several sensitivity experiments show that, with such an amplitude, the perturbed solution is reasonably divergent from the control solution after one rescaling step, and, meanwhile, the bred vectors can converge relatively quickly. The rescaling period is one month, as in [9]. With these parameters, we found that the fast instable growth can get saturated after 4–6 breeding cycles for all initial conditions in the HCM. Thus in the following analysis, we focus on the BVs at the sixth rescaling cycle.

The rescaling factor λ_k at cycle k is defined using the amplitude of the perturbation growth of averaged HCAs over the Niño3.4 region (170° W–120° W, 5°S–5° N), measured by the L-2 norm as in [9]. The Niño3.4 HCA is chosen due to its critical importance in ENSO simulation and prediction (e.g. [21]). It is found that BVs are generally insensitive to the definition of norm, unlike singular vectors (e.g. [7]). Since the initial perturbation is random, a single BV might not effectively characterize the optimal error growth due to realistic uncertainty. Therefore, one should consider using multiple pairs of random perturbations to obtain multiple BVs for each initial condition. Recently, Tang et al. [18] found that an ensemble size of 15–20 might be sufficient to measure ENSO prediction uncertainty. Also, considering the computational cost, we used 15 pairs of random perturbations for each initial condition, i.e., 15 BVs correspondingly. BVs were obtained for each variable individually. The perturbed variables include sea temperature, horizontal currents and vertical currents of the top 250 m (17 model levels). The BVs are computed every three months from January 1881 to October 2000 (i.e., January 1881, April 1881, … October 2000). Thus there are a total of 15 × 480 BVs, providing sufficient samples to perform a statistical predictability analysis.

The cumulative growth rate for bred vector m after cycle k is defined below, as in [6]:

$$G_k^m = \begin{cases} \lambda_1^m & \text{if } k = 1; \\ \lambda_k^m G_{k-1}^m & \text{if } k > 1. \end{cases}$$

G_k^m is λ_k multiplied by the previous cumulative growth rate. The averaged G_6^m over 15 BVs is referred to as the BV-rate, the average growth rate of bred vectors associated with a given initial state.

2.3. BV-dimension and BV-skewness

BV-dimension is defined here as in [4], a measure of local dimension of the bred vector subspace. Considering the importance of SST and heat content (HC) in the ENSO system, we use both SST and HC BVs to construct a joint field for BV-dimension analysis. For a given initial state, denoted by l, at which the BV is obtained, the BV-dimension is analyzed using the method proposed in [4]. First, a domain of 25 grid points (5 × 5) surrounding a model grid point j is identified, and the values of the SST and HC BVs at the 25 grid points form a 50-dimensional column vector which is referred to as a local bred vector. The model's horizontal resolution in the zonal direction is 2°, and the resolution in the meridional direction is 0.5 within 5° of the equator, smoothly changing up to 2.0° at 30° N and 30° S. Thus the domain of 5 × 5 is equivalent to 900 km by 55 km within 5° of the equator, smoothly changing up to 900 km by 900 km at the boundary of 30° N and 30° S. Sensitivity experiments show that the BV-dimension does not change much with the domain size. For example, the domain of 2.5 × 2.5 or 10 × 10 has a BV-dimension very similar to that of a 5 × 5 domain. Second, normalization is performed first for SST BVs, and then the SST is rescaled to give both HC and SST BVs the same mean-square norm. Finally, normalization is performed for both SST and HC BVs to ensure a unit magnitude of the full 50-dimensional vector. Third, there are 15 BV members for each grid; thus a matrix of size 50×15, denoted by A, is obtained. Finally, the principal component analysis (PCA) is employed for the matrix A, i.e.,

$$A * A^T \mathbf{u}_i = \sigma_i \mathbf{u}_i \tag{1}$$

where $\mathbf{u}_i$ and σ_i are the ith eigenvector and eigenvalue, respectively.

The BV-dimension ψ at grid j is defined as below: [4,6]

$$\psi_j^l = \frac{\left(\sum_{i=1}^{15} \sigma_i\right)^2}{\sum_{i=1}^{15} \sigma_i^2}. \tag{2}$$

ψ_j^l presents the variance accounted for by eigenvectors which can effectively characterize the subspace of j (i.e., the dimension). For example, if the first two σ_i^2 values are 0.50 and 0.49, the BV-dimension is close to 2 from (2); alternatively, if the first three σ_i^2 values are 0.33, 0.33 and 0.33, the BV-dimension is close to 3. Thus, ψ_j represents the effective dimension of point j. Repeating this process for all model grids, we get the BV-dimension for the whole domain, denoted by Ψ^l, for the given initial state l. Since l changes by 3-month intervals from 1881 to 2000, we have a total of 480 Ψ, denoted by Ψ^{all}. From Ψ^{all}, one can explore the effective dimension

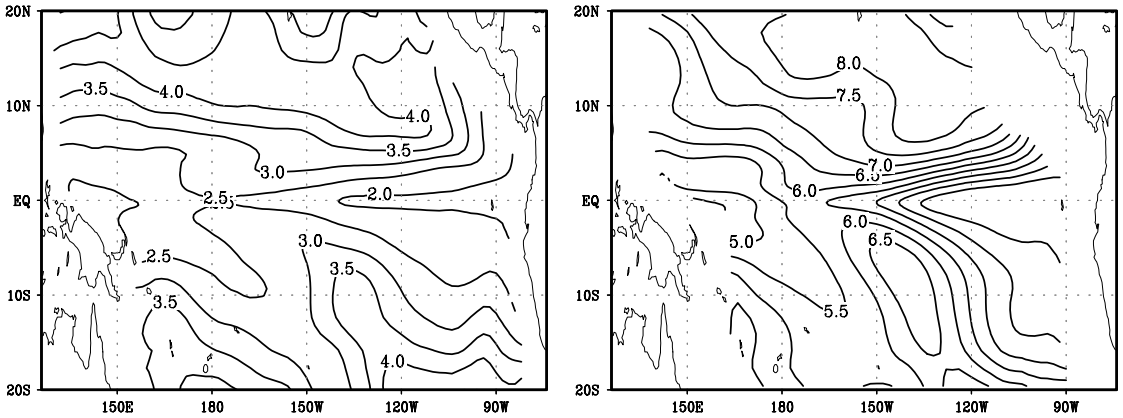

(a) Average BV-dimension. (b) BV-dimension test.

Fig. 1. (a) Average BV-dimension over all initial conditions from 1881 to 2000; and (b) BV-dimension test obtained using surrogate data (see text).

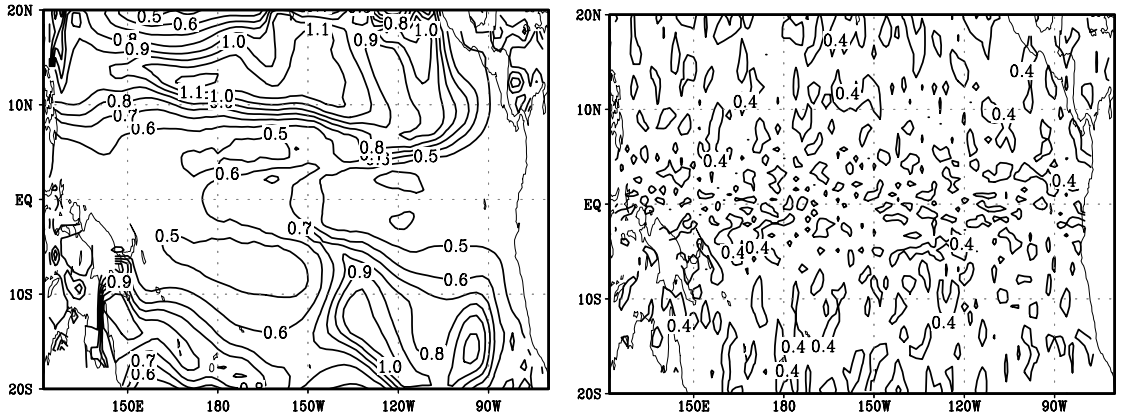

(a) BV-skewness. (b) BV-skewness test.

Fig. 2. (a) Average BV-skewness over all initial conditions from 1881 to 2000; and (b) BV-skewness test by the Monte Carlo method (see text). Non-zero values in (b) are due to sampling errors.

across the whole domain at a specific time and the evolution of the dimensional structure with time.

For a given grid point j, there are 15 values each from an individual BV. If the system is linear, the 15 BV values would be from a population of normal distribution, as the initial perturbations, with a mean of zero and a variance of constant value that is determined by the variance of initial perturbation and the amplification of the linear system. If sampling errors are ignored, the skewness of the 15 BV values will vanish. Thus, a significant non-zero skewness indicates the existence of nonlinearity. In the analysis below, we use the skewness obtained from the BV, called the BV-skewness, to characterize the nonlinearity. A significant feature of ENSO nonlinearity is the asymmetry between the El Niño and La Niña events. Often the larger the asymmetry the stronger the nonlinear behavior of ENSO.

3. Low-dimensional nonlinearity of ENSO in the BV

In this section, we will explore the low dimension and nonlinearity of ENSO using the BV-dimension and the BV-skewness as introduced above. Fig. 1(a) is the average BV-dimension Ψ^{all} over the entire period from 1881 to 2000, showing a well-defined structure. The relatively low values of the BV-dimension distribute along the equator and increase with latitude. As can be seen in Fig. 1(a), the BV-dimension ranges from 2 to 4 in the whole domain of the tropical Pacific ocean, suggesting a low-dimensional system there. This is true, in particular, for the equatorial Pacific ocean, i.e., the ENSO system, where the BV-dimension is always below 3. The low-dimensional feature of ENSO has also been noticed in previous works using fractal dimension analyses of observed data or theoretical analyses of simplified models (e.g., [16,22]). Here a similar conclusion is obtained using a completely different method, further validating the low dimension of the ENSO system.

In order to determine if the low BV-dimension regions are statistically significant and not due to random fluctuations, we apply the BV-dimension analysis to surrogate data which are not temporally correlated as in [4]. The surrogate data is generated by 15 bred vectors randomly chosen from 15 different initial conditions which are substantially far apart, and this process is repeated 1000 times. The averaged BV-dimension obtained using the 1000 surrogate data points is shown in Fig. 1(b). As can be seen, there are no values of BV-dimension less than 4, indicating that Fig. 1(a) is statistically significant.

The nonlinearity of ENSO can be characterized by the BV-skewness as argued in Section 2. The averaged BV-skewness of HCAs over the entire 120 years is shown in Fig. 2(a). The BV-skewness of SSTAs has a structure similar to Fig. 2(a). Fig. 2(b) shows a BV-skewness using a linear system instead of the HCM, which gives the estimate error due to infinite samples. The linear system is designed so that its responses to initial perturbations of BVs have the same amplitude as that of the HCM. There are no values of BV-skewness greater than 0.4 in Fig. 2(b); therefore, the value of 0.4 could be used as an upper threshold for testing in Fig. 2(a). Comparing Fig. 2(a) with Fig. 2(b) indicates that ENSO is a nonlinear system. However, the BV-skewness values in Fig. 2(a) are all in the range 0.6–0.8 in the equatorial region, not

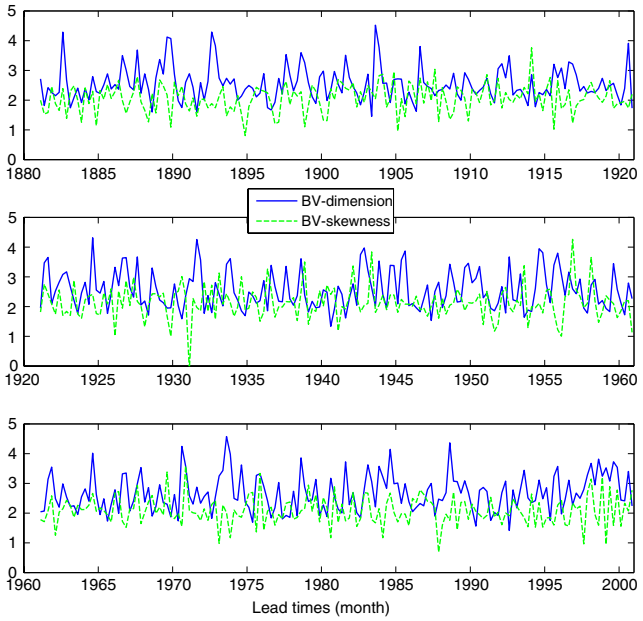

Fig. 3. Variation of BV-dimension and BV-skewness index, averaged over the Niño3.4 region. The BV-skewness is shifted by a constant value of 2 prior to plotting for better presentation.

much larger than the threshold value, suggesting that ENSO is a low-dimensional and weakly nonlinear system.

There are resemblances between the averaged BV-skewness and the averaged BV-dimension, e.g., small values along the equator and large values increasing with latitude. However, the averaged BV-skewness has two relatively large centers distributed at 15° N/S which are absent in Fig. 1. Interestingly, the feature of the averaged BV-skewness is consistent with the degree of nonlinearity measured by observations and a neural network as reported in Tang et al. [23]. In their work, the surface zonal wind, SST and HC simulations were compared between two statistical models: a nonlinear neural network (NN) and a linear regression (LR). It is found that the NN has only a slight difference from the LR along the equator but a significant difference in the region around 15° N/S. Such a consistent result between BV analysis of the HCM and these statistical analyses of observations further verify the low-dimensional and weakly nonlinear nature of ENSO.

It is meaningful to examine temporal variations in the intensity of the low-dimensional nonlinearity of ENSO. Shown in Figs. 3 and 4 are the Niño3.4 indices of BV-dimension and BV-skewness, as defined by their averaged values over the Niño3.4 region, and their wavelet power spectrums. The local wavelet power spectrums clearly indicate that the significant periods are localized in time. For the BV-dimension, the interannual variability is significant at a 2–6-year time scale for almost the entire period, as indicated in Fig. 4, whereas the decadal variability only appears in the 1880s–1900s and 1980s–1990s. For BV-skewness, the 2–7-year interannual variability is weak for the entire period from 1881 to 2000, but there is significant interdecadal variability over 10-year periods. In particular, the intraseasonal variability under 2-year periods is significant for most periods, as shown in Fig. 4. The striking intraseasonal variability of BV-skewness can also be clearly observed in Fig. 3, suggesting the nonlinear nature of the seasonal cycles and the weak nonlinearity of interannual variability.

Further analysis examines the relationship between BV-dimension and BV-skewness, and the relationship between the intensity of low-dimensional nonlinearity and ENSO variability itself. A series of correlation coefficients are calculated using Niño3.4 indices including SSTA and HCA indices. It is found that BV-dimension and BV-skewness are not statistically related to each other, and do not correlate with either the SSTA/HCA index or the amplitude (absolute value) of the SSTA/HCA index (not shown), suggesting that the intensity of ENSO variability is not dominated by its low-dimensional nonlinearity in the HCM. This result is consistent with our recent findings in the ZC model, in which the contribution of linear heating to ENSO variability is around 2–3 times as much as that of nonlinear heating [24]. However, at interdecadal time scales, we find there is a negative correlation between BV-skewness and ENSO variability obtained using a 20-year running mean approach, namely that the interdecadal variation in BV-skewness is nearly out of phase with that in ENSO variability. We will discuss this further in Section 5.2.

In summary, the BV analysis of the HCM suggests that ENSO is a low-dimensional nonlinear system. The intensity of the low-dimensional nonlinearity varies at different time scales from intraseasonal to interdecadal scales. There is no evidence of the relationship between the intensity of the low-dimensional nonlinearity and ENSO variability at the interannual time scale.

4. Low-dimensional nonlinearity of ENSO in observations

In the preceding section, we analyzed an ENSO dynamical system using the breeding method, and found that ENSO can be described as a low-dimensional nonlinear system. In this section, we will further explore the low-dimensional nonlinearity of ENSO using observations. This analysis will substantiate the above conclusions further and shed light on the ENSO mechanisms.

The first method used to detect low-dimensional nonlinearity in observations is the residual delay map (hereafter referred to as

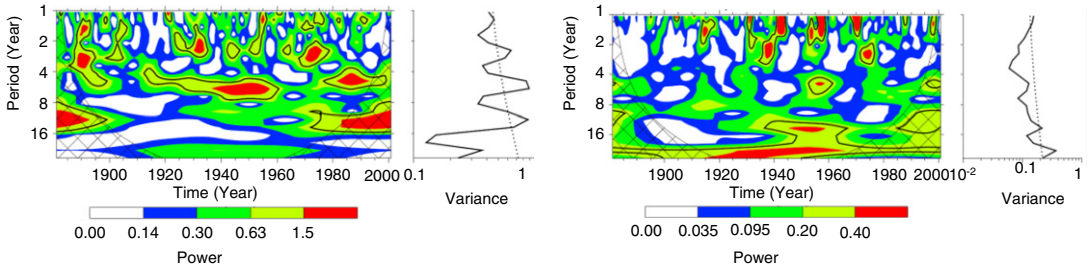

(a) BV-dimension. (b) BV-skewness.

Fig. 4. Wavelet power spectrum for (a) BV-dimension and (b) BV-skewness. The contour (boundary of two colors) levels are chosen so that 75%, 50%, 25%, and 5% of the wavelet power is above each level, respectively. The cross-hatched region is the cone of influence, where zero padding has reduced the variance. The black contour is the 5% significance level, using a red-noise (auto-regressive lag 1) background spectrum. The right panels are the global wavelet power spectrum (black line) and the significance for the global wavelet spectrum, assuming the same significance level and background spectrum (dashed line). The *y*-axis unit is a year.

RDM) proposed by Sugihara et al. [25] and Patil et al. [26]. The RDM is a lagged plot of the residual (error) against the data itself. The residual is defined as the difference between the simulation of a predictive model and the data. If a predictive model accurately describes the inherent dynamics of observed data, the residual should exhibit no relationship to the data itself. In terms of the identification of low-dimensional nonlinear components in dynamics, the predictive model should be a linear auto-regressive model [26]. In other words, if the data could be precisely described by linear processes, there should be no statistical relationship between the residual and the data itself. On the other hand, if the underlying dynamics inherent to the data has a sufficiently large dimension, the data should appear to be noise resulting in no observed relationship in the RDM either. However, if there are low-dimensional nonlinear processes that are dominating the dynamics, then a nonlinear statistical relationship may be observed in the RDM, indicating that the linear predictor could be improved by adding nonlinear terms [26].

An issue in the RDM is the bin size N, which is used to sort the residual and the data. To obtain a stable and observed relationship in the RDM, the averaged values (residual and the data itself) of each bin are plotted instead of individual values at each time point. A larger N is likely to make the structure of the RDM more stable and easily observed, but could lead to few samples and distort the relationship in the RDM, whereas a smaller N could cause the sampling noise to contaminate the relationship. In this study, we will empirically determine the N through sensitivity experiments as in [26]. The empirical approach is also applied to determine the order of the linear auto-regressive model.

The RDM obtained using the time series of the first POPs (Principal Oscillation Patterns [27]) mode derived from a joint field of HC and SST is shown in Fig. 5(a). The SST data is the monthly Extended Reconstruction version 2 SST (ERSST.v2) dataset from 1881 to 2000, reconstructed by Smith and Reynolds [28] with a resolution of 2° × 2°. The HC is a reanalysis dataset from 1881 to 2000, obtained using the OGCM and SST assimilation by Tang et al. [18] (available from http://web.unbc.ca/ytang/wind.html). We use both SST and HC to characterize ENSO due to their importance in ENSO variability (e.g. [21]). In contrast to the classic principal component analysis which describes the stationary patterns that account for different fractions of the variance, POPs describe the oscillatory behavior of the field, thus better characterizing the behavior of ENSO and its dynamics. In Fig. 5(a), the order of the auto-regression model is 3 and the bin size is 12. However, the variations in the order from 2 to 10 and in the bin size from 6 to 24 result in little change in the RDM structure.

The parabola-like structure shown in Fig. 5(a) is the optimal fit of the residual against the data using a quadratic function, which is statistically significant at the confidence level of 95%, indicating that the underlying dynamical process is inherently low-dimensional and nonlinear. Fig. 5(b) is an RDM using surrogates of the original data, constructed by a Fourier transform [26]. The surrogate data has the same autocorrelation as the original data but only preserves the linear components. The RDM shown in Fig. 5(b) is used to examine if Fig. 5(a) could be randomly obtained, and thus be not statistically significant. As can be seen in Fig. 5(b), the parabola-like structure seen in Fig. 5(a) is not present since there is no longer a nonlinear component in the dynamics. The visible differences between the two figures verify the low-dimensional nonlinearity shown in Fig. 5(a).

The low-dimensional nonlinearity of ENSO can be further diagnosed by analysis of the correlation dimension, which is a characteristic measurement of strange attractors. The dimension, d, of a strange attractor indicates the minimum number of variables that are necessary to describe a system's evolution in time. The correlation dimension has been widely used in studying the chaotic characteristics of atmospheric phenomena (e.g. [29,30]).

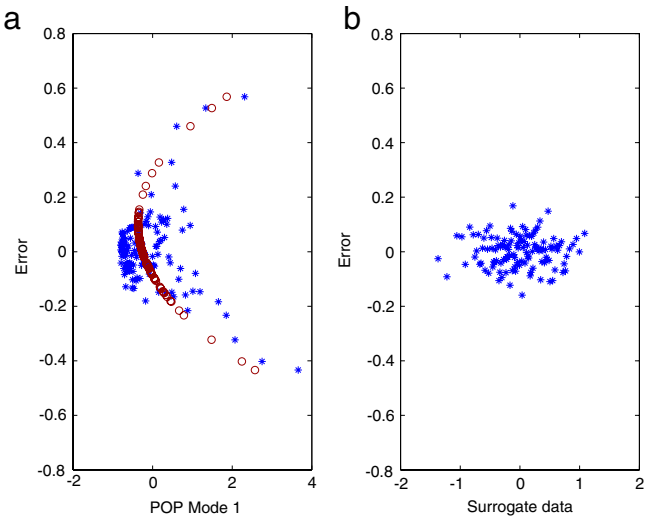

Fig. 5. (a) RDM using a linear predictive model of POPs time series from 1881 to 2000 (asterisk). The circle is the optimal fit by a quadratic function using the least-squares method; (b) the same as (a) but using surrogate data.

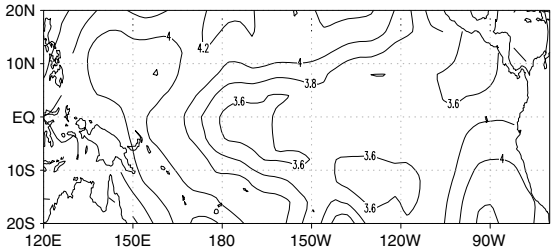

Fig. 6. Correlation dimension of SSTA from 1881 to 2000.

Given a time series x_i, $i = 1, \ldots, T$, a state space vector X_t is constructed by $X_t = [x_t, x_{t+\tau}, \ldots, x_{t+(m-1)\tau}]$, where τ is the delay time, and the dimension m of the vector is known as the embedding dimension. Thus, the correlation integral is [31]

$$C(r) = \frac{2}{N(N-1)} \sum_{j=1}^{N} \sum_{i=j+1}^{N} \Theta(r - |X_i - Xj|). \tag{3}$$

Here N is the size of X_t, and Θ is the Heaviside function defined by $\Theta(s) = 0$ for $s \leq 0$ and $\Theta(s) = 1$ for $s > 0$. The double sum counts the number of pairs (i, j) with a distance $|X_i - Xj|$ less than r. Thus the correlation dimension is approximated by

$$d = \frac{\log C(r)}{|\log r|}. \tag{4}$$

Shown in Fig. 6 is the correlation dimension d of the monthly SSTA from 1881 to 2000. Sensitive studies show that when r varies within a range 0.1 °C–0.5 °C, the delay time is 7 months and the embedding dimension is also equal to 7 ($m = 7$), so the correlation dimensions converge to the values given in Fig. 6. The structure of the correlation dimension is similar to the BV-dimension as shown in Fig. 1(a), with relatively low values in the equatorial central and eastern Pacific. The dimension number is in the range 3–4, suggesting low-dimensional nonlinearity for ENSO. The dimension number of Fig. 6 is a little larger than that in Fig. 1(a), probably because the actual observation is more complex than the model. A similar result can be obtained using HCA data. Thus the diagnosis of observations verifies the low-dimensional nonlinearity as found in the above BV analysis.

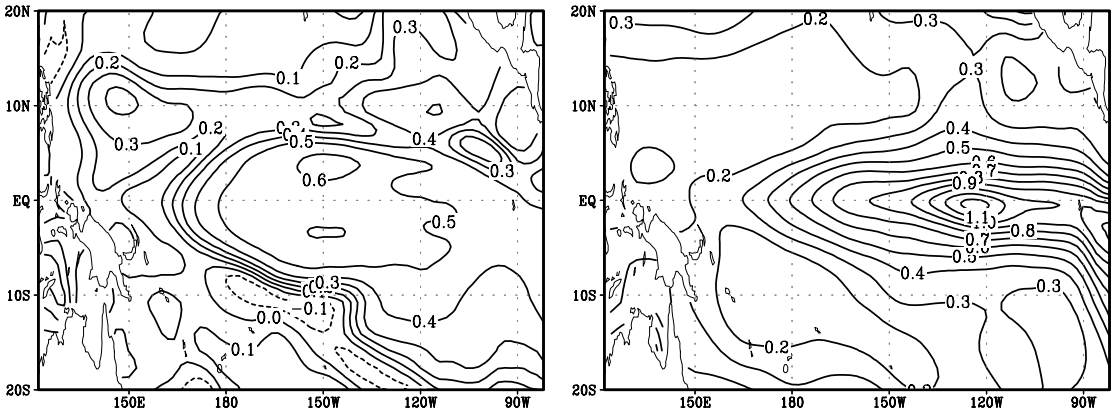

(a) Correlation skill. (b) RMSE skill.

Fig. 7. (a) Correlation skill of predicted SSTAs against the observed counterpart for the period from 1881 to 2000 for the tropical Pacific, averaged over lead times of 1–12 months; (b) the same as (a) but for the RMSE.

5. Impact of low-dimensional nonlinearity of ENSO on its predictability

5.1. BV-skewness and predictability

In this section, we will examine the impact of intensity of low-dimensional nonlinearity on ENSO predictability and their relationship on decadal/interdecadal time scales. A retrospective ENSO prediction is performed for the period from 1881 to 2000 using the HCM. A total of 480 forecasts, initialized from January 1881 to October 2000, are run starting at 3-month intervals (1 January, 1 April, 1 July, 1 October), and continued for 12 months for the HCM. The SST assimilation is performed to initialize the forecasts as described in Section 2.1.

Shown in Fig. 7 are the correlation and RMSE (root-mean-square error) skills of the predicted tropical Pacific SSTAs against the observed counterparts, for the period from 1881 to 2000, averaged over lead times of 1–12 months. The correlation skills are manifested mainly in the equatorial central and eastern Pacific like many ENSO models (e.g., [32,18,13]), decreasing towards the west and higher latitudes. The maximum RMSE occurs in the equatorial eastern Pacific, associated with the high variance in the region. Fig. 7 is similar to the pattern of potential predictability of the tropical SST obtained using a nonlinear Lynapunov exponent [33].

Comparing Fig. 7(a) with Fig. 2(a) reveals good prediction skills occurring in the equatorial region where there is a low center of BV-skewness. This suggests an inverse relationship between prediction skill and BV-skewness. A strong nonlinear system is usually less predictable due to unpredictable chaotic components. In the following sections, we will show further evidence of the inverse relationship. Fig. 2 sheds light on some reasons why almost all ENSO prediction models have the best prediction skill in the equatorial central Pacific, and why the potential predictability of SSTAs is the highest in the region [33]. However, there is inconsistency between the BV-skewness and predictability in the region around 180W/5S-10S, suggesting that the SST predictability is not much dominated by the nonlinear strength in this region where stochastic forcing such as WWB (westerly wind burst) is strong. A linear system, when forced by stochastic forcing (such as white noise), has small skewness and poor predictability.

Fig. 7 is an averaged skill over the lead time of 1–12 months. We address the average skill in this study considering the following. (i) The averaged skill measures an overall predictability of the entire lead times, as a function of initial conditions (i.e., reference trajectory of BV analysis). It is a major interest to examine the overall predictability due to initial uncertainty that is inherent to BV analysis in this study. (ii) It avoids the somehow artificial choice of a specific lead time (e.g., 3-month lead or 6-month lead or others). It should be noticed that the prediction skill decreases smoothly with lead times, but the spatial distributions at individual lead times are very similar to one another, and to Fig. 7, as shown in Figs. 8 and 9. Actually the findings and conclusions from the averaged skill are similar to those from skills at a specific lead time.

Fig. 10 shows the averaged correlation (R) and RMSE skill of the Niño3.4 SSTA index over 1–12 month leads, measured by a running window of 20 years from 1881 to 2000 (i.e., 1881–1900, 1882–1901, 1883–1902, ..., 1980–1999, 1981–2000).[1] For comparison, the averaged Niño3.4 BV-skewness index over the running window is also plotted in Fig. 10 (green line). As can be seen, the prediction skills show a pronounced interdecadal variation. Generally good skills appear in the periods around 1881–1900 and 1961–2000, whereas poor skills occur during the period from 1910 to 1960. Such an interdecadal variation is also found in other ENSO models ([13,18]). Of interest, the BV-skewness index also shows a visible interdecadal variation that is inversely related to that of prediction skills. The correlations of BV-skewness index to R and the RMSE are −0.60 and 0.64, respectively; i.e., the smaller the BV-skewness, the larger the R and the smaller the RMSE. Fig. 10 suggests a possible interpretation of the interdecadal variation in ENSO predictability, namely, as the ENSO cycle resides in a phase that has a relatively low BV-skewness (i.e., weak nonlinearity), it is more predictable, and vice versa. Thus one might be able to argue that the interdecadal variation in ENSO predictability is due mainly to variation in the intensity of low-dimensional nonlinearity. This interpretation might complement a well-proposed mechanism of decadal variability in ENSO predictability, namely, the variations in predictability are probably due to variations in ENSO variability (e.g. [34,35,13,18,20]). Tang et al. [18] recently found in several models that the period with strong ENSO signals often had invariably high predictability, and vice versa. The intensity of ENSO signals may be dominated by the linear components of the ENSO system as argued in some works (e.g., [19,24]). Therefore a period that covers strong ENSO signals probably has relatively weak nonlinearity, leading to high predictability. As argued in the Introduction, there are two kinds of source in general that limit ENSO predictability: the chaotic behavior of the nonlinear dynamics of

[1] The overall skill measured during a 20-year window is plotted at the middle point of the window in Fig. 2, where the predicted Niño3.4 SSTA is compared against the observed value. For example, the skill at 1890 is calculated using the samples from 1881 to 1900. The 20-year window is shifted by one year each time starting from 1881 until 2000.

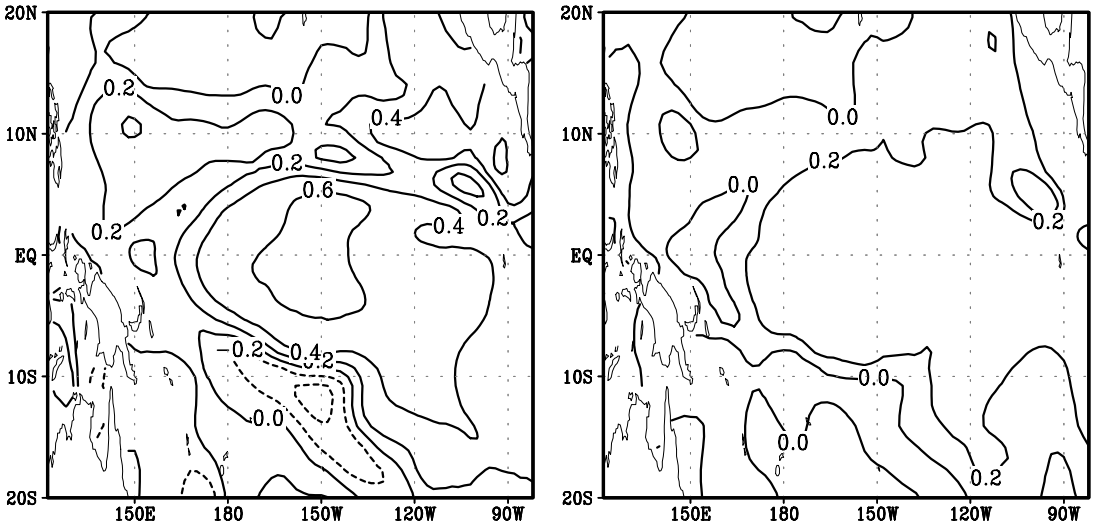

(a) 6-month correlation. (b) 12-month correlation.

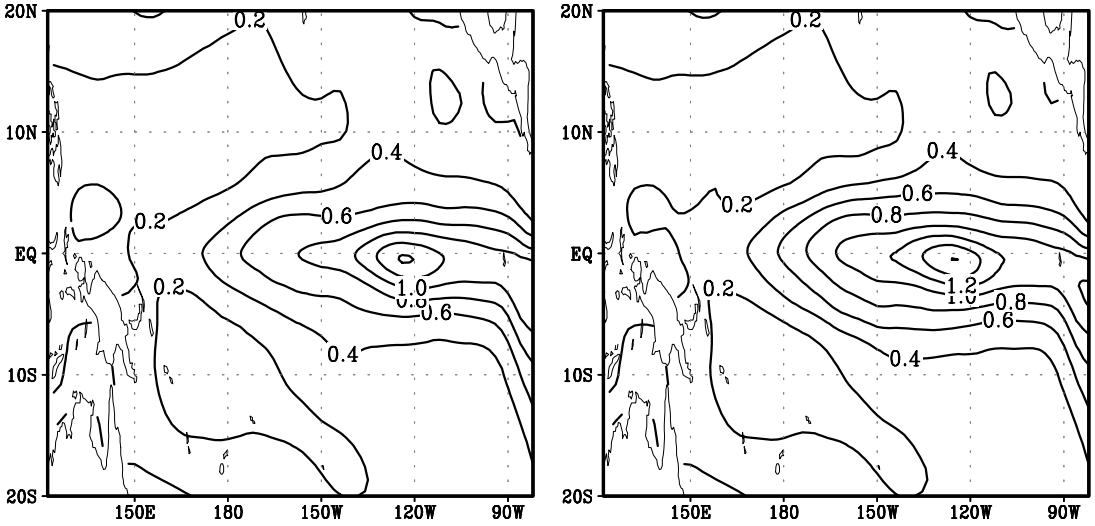

(c) 6-month RMSE. (d) 12-month RMSE.

Fig. 8. The same as Fig. 7 but for lead time of 6 months (a and c), and 12 months (b and d), respectively.

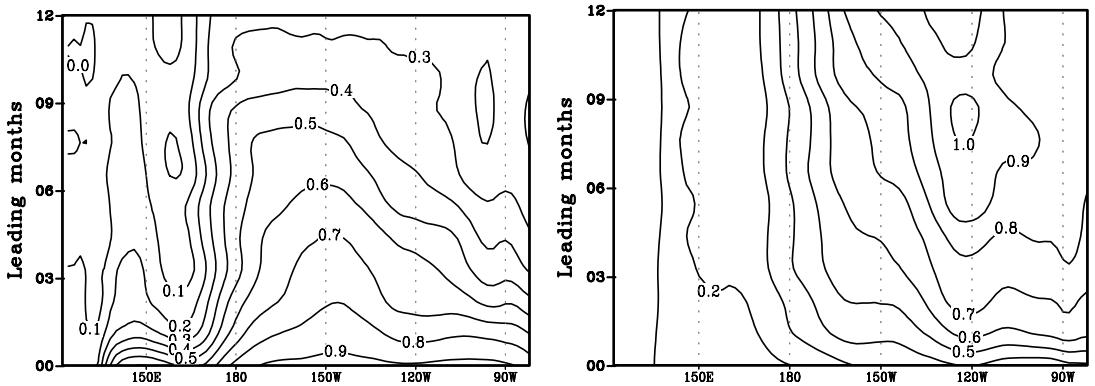

(a) Correlation skill. (b) RMSE skill.

Fig. 9. (a) Correlation skill of predicted SSTAs against the observed counterpart for the period from 1881 to 2000, averaged over 5S-5N, as a function of leading time and longitude. (b) The same as (a) but for the RMSE.

the coupled system (e.g. [12,13]); and the stochastic nature of the coupled system characterized by weather noise and other high-frequency variations. Our analysis seemingly supports the stochastic nature theory of ENSO predictability. In other words, ENSO is a low-dimensional weak nonlinear system in which the stochastic noise limits its predictability. As the strength of nonlinearity weakens, the ENSO signal is inversely enhanced, which is more able to "resist" dissipation of signal components by the stochastic noise.

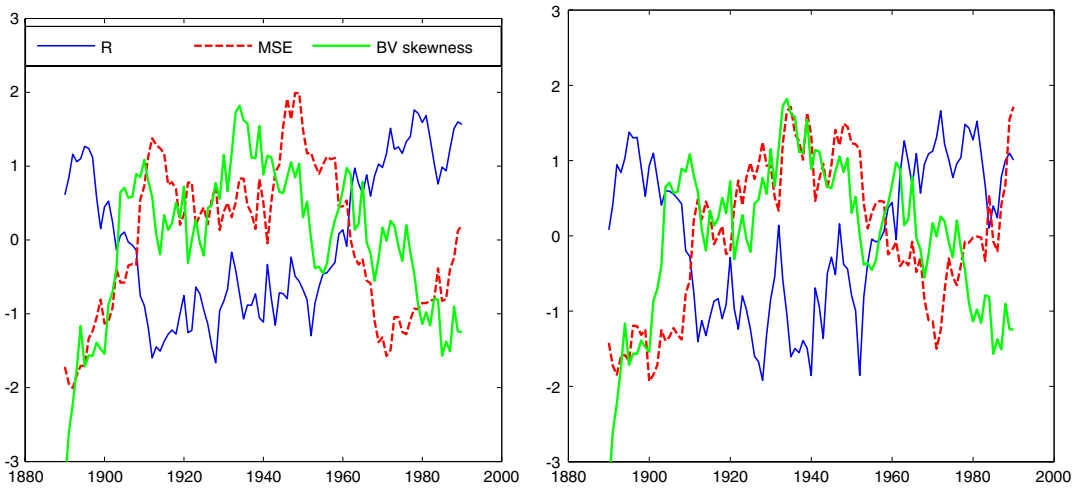

(a) BV and the average predictability. (b) BV and 6-month predictability.

Fig. 10. The average of the anomaly correlation R (black) and RMSE (dashed) between the observed and the predicted Niño3.4 SSTA indices over lead times of 1–12 months. The correlation R and the RMSE are computed at each running window of 20-year periods from 1881 to 2000 (see text). The average BV-skewness over each window is plotted as a gray solid line. Normalization was done for each dataset prior to plotting.

A similar analysis was also performed for the BV-dimension Nino3.4 index and predictability (not shown). Interestingly, the BV-dimension Nino3.4 index shows a visible interdecadal variation that tends to be inversely related to the variation in prediction skills, namely, smaller BV-dimension values have relatively lower predictability. It is unclear why they have an inverse relationship. One possible reason is that ENSO is always a low-dimensional and weakly nonlinear system, as argued above. A low-dimensional and weakly nonlinear system might have better predictive skill when more variables are used to describe (predict) it.

The good relationship between predictability and BV-skewness can be further demonstrated in Fig. 11, where the R and RMSE are measured for each individual initial condition from 1881 to 2000, i.e., predicted Niño3.4 index against the observed counterpart over 12-month leads. A running mean of 20 years is applied to the 480 R and RMSE values as well as the Niño3.4 BV-skewness index to alleviate the impact of individual cases. As shown in Fig. 11, there is a good inverse relationship of BV-skewness to R and the RMSE. As the BV-skewness is large the skills are poor, whereas good skills appear only when the BV-skewness is small. For example, when the BV-skewness is smaller than 0.1, both R is large and the RMSE is small.

In summary, there is a significant inverse relationship between BV-skewness and ENSO predictability at decadal/interdecadal time scales. The small value of BV-skewness leads to good predictability, and vice versa.

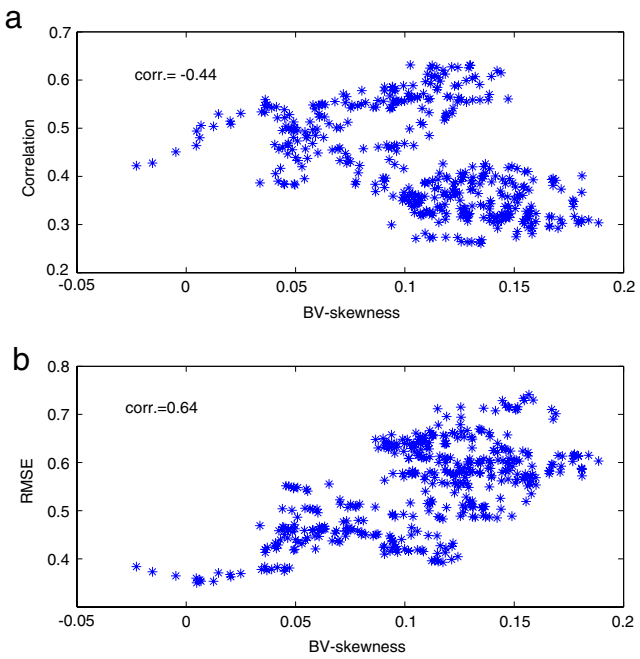

Fig. 11. Scatter plot of prediction skill: (a) R and (b) the RMSE of each individual forecast against the BV-skewness for the period from 1881 to 2000.

5.2. BV-skewness and BV growth rate

The BV-rate, as defined in Section 2.2, measures the cumulative growth of initial errors (perturbations) from initial time until the fast instable growth is saturated. Conceptually, the BV-rate might be inherently related to BV-skewness and predictability. Shown in Fig. 12 are variations in BV-rate and BV-skewness from 1881 to 2000, obtained using 20-year running mean windows in order to address their decadal/interdecadal variability. A positive correlation of 0.38 can be obtained between the BV-rate and BV-skewness for the entire period, but their relationship varies in three different periods: the 1890s–1920s, the 1960s–1990s and the 1930s–1950s, as seen in Fig. 12 and indicated by their correlation coefficients of 0.80, 0.67 and −0.85. Comparing Fig. 12 with Fig. 10 reveals that the BV-rate is not always a good indicator of predictability. If the BV-rate is positively related to the BV-skewness, it is a good measure of predictability as observed for the periods 1890–1910 and 1960–2000. However, if the BV-rate has an inverse relationship with the BV-skewness, the BV-rate is not effective in measuring predictability, as in the period 1920–1960 when a small BV-rate and a low predictability occur simultaneously. Thus a small BV-rate is not always necessarily associated with a high predictability.

Intuitively, a small BV-skewness reflects low-dimensional weak nonlinearity, resulting in a small BV-rate. Thus an interesting question is why the BV-rate can be small when the BV-skewness is relatively large. This is most probably related to the fact that the value of BV-rate is determined by both linear and nonlinear physical processes of the system. It is possible that the BV-rate is still large if the contribution of the nonlinear process is small but the contribution of the linear process is large. Thus, the BV-rate could be more dominated by the linear process in some periods than in other periods, in which case the role of the nonlinear

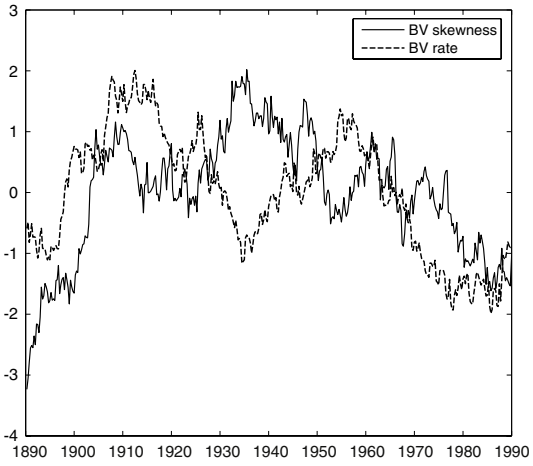

Fig. 12. Normalized BV-skewness and BV-rate from 1881 to 2000. The 20-year running mean is applied to reflect the decadal/interdecadal variability in BV-rate and BV-skewness.

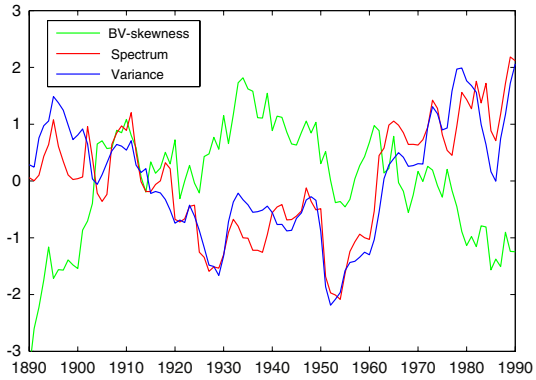

Fig. 13. BV-skewness (black) and the strength of ENSO signals measured by both the power spectrum of ENSO frequencies at 2–5-year periods (gray dotted) and the variance (gray dashed). The intensity of the signals was estimated using the observed Niño3.4 SSTA index in each running window of 20 years from 1881 to 2000.

process in the BV-rate is negligible. This might explain why the BV-rate is not always effective in measuring the predictability, since it is the nonlinear process that limits the predictability, as evidenced by the good relationship between BV-skewness and predictability. In other words, it is the nonlinear component of the BV-rate, not the total BV-rate, that characterizes the predictability well.

This result is consistent with our recent work using the ZC model [24], where the optimal error growth rate (the first singular value) is found to result from linear dynamical heating and nonlinear dynamical heating. The contribution of linear dynamical heating to the optimal error growth rate is about twice as much as that of nonlinear dynamical heating for 1881 to 2000, but the predictability is much better reflected by the latter. In other words, ENSO predictability is mainly determined by the nonlinear process, even though the nonlinearity may be neither strong nor high-dimensional. Nonlinear effects on ENSO have been widely discussed (e.g., [36–38,21,39]). Jin et al. [40] and An and Jin [36] pointed out that the nonlinear dynamical heating could play an important role in the asymmetry between amplitudes of El Niño and La Niña events, which affect the potential predictability.

A good relationship between the intensity of the ENSO signal and predictability has been reported recently (e.g., [13,41,42,18]). It was argued that the strong ENSO signal is probably due mainly to the contribution from the linear dynamical process (e.g. [24,23, 21]). In the ZC model, the contribution of linear heating to the ENSO signal is about 2–3 times that of nonlinear heating. The dominant role of the linear dynamics in the ENSO system does not conflict with the aforementioned conclusion that the nonlinear process is a major source to limit ENSO predictability. A period with stronger ENSO signals might contain a stronger linear process and a relatively weaker nonlinear process, leading to higher predictability. Fig. 13 shows the decadal/interdecadal variation in BV-skewness and in the intensity of ENSO signals that was measured by both the variance and power spectrum at frequencies 2–5 years of the observed Nino3.4 SSTA index in each 20-year running window., As can be seen, strong ENSO signals often correspond with low BV-skewness, with correlation values of −0.49 and −0.43 of BV-skewness to the variance and to the power spectrum, respectively. Comparison between Figs. 13 and 10 reveals a good link between the ENSO signal, BV-skewness and predictability, as argued above.

Fig. 14 further shows the connection between the ENSO signal and the linear process, where a linear auto-regression model is used to simulate the Niño3.4 SSTA index. As can be seen, the simulation error is not significantly larger for stronger signals. For example, for very strong events, say Niño3.4 SSTAs greater than

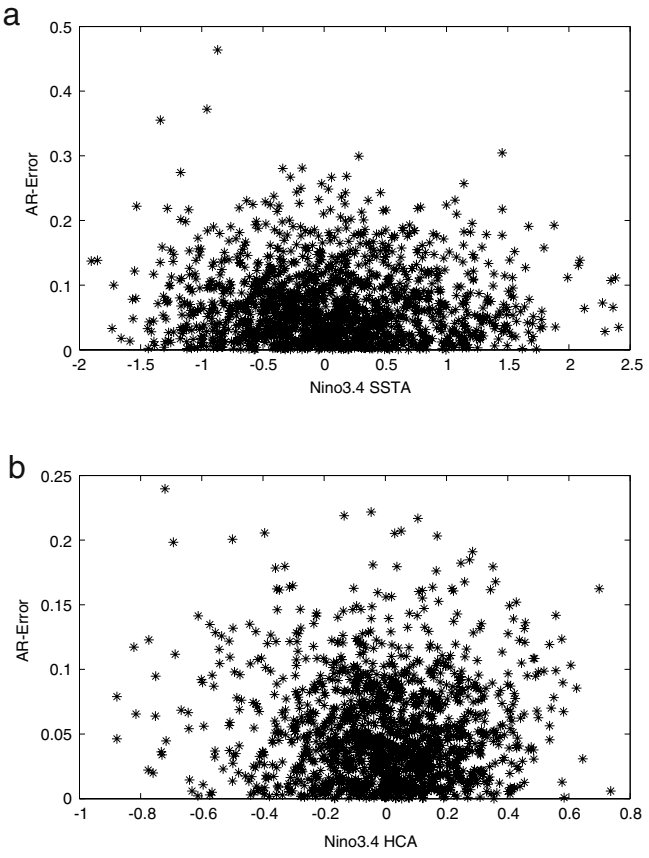

Fig. 14. (a) The prediction errors of the Niño3.4 SSTA index, obtained using the second-order auto-regression prediction model, against the observed counterpart; and (b) the same as (a) but for the HCA index.

2.0 °C, the simulation errors are not relatively larger. If several points (outliers) are excluded, the error distribution is actually bounded by a semi-circle for both SST and HCAs. This example suggests that the low-dimensional nonlinearity of ENSO, rather than its linearity, is a major source that limits its predictability. It should be noted that the nonlinearity associated with the asymmetry between El Niño and La Niña events, as noted in many studies (e.g., [36,18]), is not equivalent to the concept of nonlinearity used in this study. The former nonlinearity focuses on the differ-

ence between ENSO events, whereas the latter only considers the evolution of SSTAs in several months.[2]

In summary, the strength of the low-dimensional nonlinearity of the ENSO system characterized by BV-skewness can greatly impact ENSO predictability. When the BV-skewness is small the predictability is high, and vice versa. In particular, when the nonlinearity is relatively weak, there is a good relationship between the BV-rate and BV-skewness, whereas when the nonlinearity is relatively strong, there is an inverse relationship between the BV-rate and BV-skewness.

6. Discussion and summary

It has been a challenge to identify the sources and processes that limit the predictability of ENSO. Nonlinearity and stochastic noise are generally thought of as the two most probable factors that limit ENSO predictability. In this study, we explored the low-dimensional nonlinearity of ENSO by applying the breeding method to a hybrid coupled model for the period from 1881 to 2000. Several important derivatives of BV analysis are examined in detail, including BV-dimension, BV-skewness and BV-rate. The results show that ENSO is a low-dimensional and weakly nonlinear system and that its nonlinear strength can be measured by BV-skewness. The low-dimensional nonlinearity of ENSO is further validated by observed data.

To explore ENSO predictability, we performed a retrospective ENSO prediction for the period from 1881 to 2000. The relationship between the intensity of low-dimensional nonlinearity of ENSO and its predictability is investigated. It is found that the BV-skewness, which does not make use of observations, has a good relationship with the ENSO prediction skill measured by the correlation coefficient and the RMSE, which make use of observations. Generally, when a period has a relatively small BV-skewness, it also has a high ENSO predictability. There is a consistent interdecadal variation in prediction skill and in BV-skewness. In the late 19th and the late 20th centuries, the BV-skewness of the ENSO background was small and the model showed high correlation skill and low RMSE, whereas during periods of high BV-skewness the model showed coincidentally poor prediction skill. Such a good relationship between the BV-skewness of the background and ENSO predictability is probably due to the critical role of the nonlinear process in limiting ENSO predictability. When the nonlinearity of the ENSO background is weak, the error growth rate due to the nonlinearity is small, leading to high predictability, and vice versa.

The optimal error growth rate is generally controlled by both linear and nonlinear dynamical processes. It was found that the nonlinear component of the BV-rate, i.e., the contribution of the nonlinear process to the BV-rate, dominates the ENSO predictability, whereas the linear component of the BV-rate is likely to be a minor indicator of predictability. This is probably because the linear errors have little impact on the correlation skill of prediction and could be alleviated in an ensemble run. Thus, an important finding in this study is that the BV-skewness, a measure of error growth associated with a nonlinear process, is a better indicator of predictability.

In this study, the low-dimensional nonlinearity of ENSO is identified using a BV analysis of the model ensemble and actual observations. This sheds some light on the ENSO mechanisms. Typically there are two mechanisms for ENSO, linear stochastic theory and nonlinear chaotic theory, partly explaining ENSO behaviors and features. This study supports an alternative mechanism, namely that ENSO is a low-dimensional and weakly nonlinear system but one which could be driven by a stochastic process. This might well explain the ENSO asymmetric and irregular features as well as the fact that low-order nonlinear even linear models can predict ENSO reasonably well (e.g., [21]).

Several cautions should be borne in mind. First, the model used in this study is a hybrid model, lacking some necessary physical and dynamical processes existing in the real world such as MJO–ENSO interaction and the impact of westerly wind burst on ENSO. In particular, the linear atmosphere used in this HCM might not be able to facilitate the advantage of the BV method very efficiently. As argued by Toth and Kalnay [1], the concept behind the breeding technique is that the saturation rates of the nonlinear growing errors characterized by different nonlinear instabilities are distinct. It will be interesting to explore whether the results and findings presented in this study also exist in complicated GCM models. Second, some of the results obtained are based on the analysis of a running window or a running mean of 20 years. The window length of 20 years is arbitrary and motivated by previous work (e.g., [13,18]). We also performed several sensitivity experiments, with the window lengths of 10 years and 30 years. The relationships between predictability and BV-skewness are similar to those presented in this paper. However, the running mean method could bring some artificial components to the correlation coefficient. Third, in this study, ENSO predictability was studied via exploring the model retrospective prediction skills. This approach assumes the model to be perfect, which is a widely used strategy in studying statistical predictability, especially the predictability due to initial uncertainty (e.g., [18]). However, no model is perfect;, therefore some features of predictability characterized by the model prediction skill might be model dependent and impacted by initial conditions, forcing and parameterization of physical processes. Finally, we applied the RDM method on the leading mode of a POPs analysis to detect the low-dimensional nonlinearity of ENSO in observations. It is unclear how the reduction of the dimension of the data impacts on the analysis of underlying dynamical dimensionality, although both are different in concept. The dimension of data here refers to the spatial domain (the number of grids) covered by the dataset whereas the latter means the minimum number of variables to describe a dynamical system. Nevertheless, it has been recognized that the leading POP mode can well characterize ENSO variability and its dynamical features (e.g. [43,21]), which should allow us to use it to detect the low-dimensional nonlinearity of ENSO.

Acknowledgements

This work is supported by the Canadian Foundation for Climate and Atmospheric Sciences (CFCAS) through Grant GR-7027 and Canada Research Chair is solo in Canada like NSF in US Canada Research Chair program.

References

[1] Z. Toth, E. Kalnay, Ensemble forecasting at NMC—the generation of perturbations, Bull. Amer. Meteorol. Soc. 74 (1993) 2317–2330.
[2] Z. Toth, E. Kalnay, Ensemble forecasting at NCEP and the breeding method, Mon. Weather Rev. 125 (1997) 3297–3319.
[3] P.L. Houtekamer, J. Derome, Prediction experiments with two member ensembles, Mon. Weather Rev. 122 (1994) 2179–2191.
[4] D. Patil, B. Hunt, E. Kalnay, J. Yorke, E. Ott, Local low dimensionality of atmospheric dynamics, Phys. Rev. Lett. 86 (2001) 5878–5881.
[5] M. Corazza, E. Kalnay, D.J. Patil, S.C. Yang, R. Morss, Use of the breeding technique to estimate the structure of the analysis error of the day, Nonlinear Process. Geophys. 10 (2003) 1–11.
[6] R.M.B. Young, P.L. Read, Breeding and predictability in the baroclinic rotating annulus using a perfect model, Nonlinear Process. Geophys. 15 (2008) 469–487.
[7] M. Cai, E. Kalnay, Z. Toth, Bred vectors of the Zebiak–Cane model and their application to ENSO predictions, J. Clim. 16 (2003) 40–56.
[8] S.E. Zebiak, M.A. Cane, A model El Niño-Southern Oscillation, Mon. Weather Rev. 115 (1987) 2262–2278.

[2] For example, for a period of 10 years, there are probably strong El Niño and La Niña events that occurred, leading to a large skewness value. This skewness value could be a measure of nonlinearity of the 10-year period. However, it is not the nonlinearity that occurs in the evolution of SSTAs of several months, which is the targeted issue of predictability studies, and defined by BV-skewness in this study.

[9] S.-C. Yang, M. Cai, E. Kalnay, M. Renecker, G. Yuan, Z. Toth, ENSO bred vectors in coupled ocean–atmosphere general circulation models, J. Clim. 19 (2006) 1422–1436.
[10] G. Gyarmati, I. Szunyogh, D.J. Patil, Local predictability in a simple model of atmospheric balance, Nonlinear Process. Geophys. 10 (2003) 183–196.
[11] G. Francisco, P. Muruganandam, Local dimension and finite time prediction in spatiotemporal chaotic systems, Phys. Rev. E 67 (6) (2003) 066204.
[12] F.-F. Jin, J.D. Neelin, M. Ghil, El Nio on the devil's staircase: Annual subharmonic steps to chaos, Science 264 (1994) 70–72.
[13] D. Chen, M.A. Cane, A. Kaplan, S.E. Zebiak, D. Huang, Predictability of El Niño in the past 148 yrs, Nature 428, 733–736.
[14] C. Penland, P.D. Sardeshmukh, The optimal growth of tropical sea surface temperature anomalies, J. Clim. 8 (1995) 1999–2024.
[15] R. Kleeman, A.M. Moore, A theory for the limitation of ENSO predictability due to stochastic atmospheric transients, J. Atmospheric Sci. 54 (1997) 753–767.
[16] A. Moore, J. Zavala-Garay, Y. Tang, R. Kleeman, J. Vialard, A. Weaver, K. Sahami, D.L.T. Anderson, M. Fisher, Optimal forcing patterns for coupled models of ENSO, J. Climate 19 (2006) 4683–4699.
[17] G. Gebbie, I. Eisenman, A. Wittenberg, E. Tziperman, Modulation of westerly wind bursts by sea surface temperature: A semi-stochastic feedback for ENSO, J. Atmospheric Sci. 64 (2007) 3281–3295.
[18] Y. Tang, Z. Deng, X. Zhou, Y. Cheng, D. Chen, Interdecadal variation of ENSO predictability in multiple models, J. Clim. 21 (2008) 4811–4833.
[19] Z. Deng, Y. Tang, X. Zhou, Long-term ENSO hindcast in a hybrid coupled model (I): SST assimilation with Ensemble Kalman filter, Clim. Dyn. (2008) doi:10.1007/s00382-008-0399-1.
[20] Z. Deng, Y. Tang, Reconstructing the past wind stresses over the tropical Pacific Ocean from 1875 to 1947, J. Appl. Meteorol. Clim. (2009) doi:10.1175/2008JAMC2049.1.
[21] Y. Tang, Hybrid coupled models of the tropical Pacific– Interannual variability, Clim. Dyn. 19 (2002) 331–342.
[22] H.A. Dijkstra, The ENSO phenomenon: Theory and mechanisms, Adv. Geosci. 6 (2006) 3–15.
[23] Y. Tang, W.W. Hsieh, B. Tang, K. Haines, A neural network atmospheric model for hybrid coupled modelling, Clim. Dyn. 17 (2001) 445–455.
[24] Y. Cheng, Y. Tang, X. Zhou, P. Jackson, D. Chen, Further analysis of singular and ENSO predictability from 1876–2003—Part I: Singular vector and the control factors, Clim. Dyn. (2009). doi:10.1007/s00382-009-0595-7.
[25] G. Sugihara, M. Casdagli, E. Habjan, D. Hess, G. Holland, P. Dixon, Residual delay maps unveil global patterns of atmospheric nonlinearity and produce improved local forecasts, Proc. Natl. Acad. Sci. 96 (14) (1999) 210–214. 215.
[26] D. Patil, B. Hunt, J. Carton, Identifying low-dimensional nonlinear behavior in atmospheric data, Mon. Weather Rev. 129 (2001) 2116–2125.
[27] K. Hasselmann, PIPs and POPs: The reduction of complex dynamical systems using principal interaction and oscillation patterns, J. Geophys. Res. 93 (1988) 11015–11021.
[28] T.M. Smith, R.W. Reynolds, Improved extended reconstruction of SST (1854–1997), J. Clim. 17 (2004) 2466–2477.
[29] A. Kawamura, A.I. McKerchar, R.H. Spigel, K. Jinno, Chaotic characteristics of the southern oscillation index time series, J. Hydrol. 204 (1998) 168–181.
[30] H.N. Shirer, C.J. Fosmire, R. Wells, L. Suciu, Estimating the correlation dimension of atmospheric time series, J. Atmospheric Sci. 54 (1997) 211–230.
[31] P. Grassberger, I. Procaccia, Measuring the strangeness of strange attractors, Physica D 9 (1983) 189–208.
[32] Y. Tang, W.W. Hsieh, Hybrid coupled models of the tropical Pacific–ENSO prediction, Clim. Dyn. 19 (2002) 343–353.
[33] J. Li, R. Ding, Temporal–spatial distributions of potential predictability of SST, J. Phys. Oceanogr. (2008) (submitted for publication).
[34] B. Wang, Interdecadal changes in El Niño onset in the last four decades, J. Clim. 8 (1995) 267–285.
[35] Y. Zhang, J.M. Wallace, DS Battisti, ENSO-like interdecadal variability: 1900–93, J. Clim. 10 (1997) 1004–1020.
[36] S.I. An, F.-F. Jin, Nonlinearity and asymmetry of ENSO, J. Clim. 17 (2004) 2399–2412.
[37] S.I. An, Interdecadal changes in the El Niño–La Nina asymmetry, Geophys. Res. Lett. 31 (2004) L23210. doi:10.1029/2004GL021699.
[38] P. Chang, L. Ji, H. Li, M. Flügel, Chaotic dynamics versus stochastic process in El Nio-Southern oscillation in coupled ocean–atmosphere models, Physica D 98 (1996) 301–320.
[39] F. Eccles, E. Tziperman, Nonlinear effects on ENSO's period, J. Atmospheric Sci. 61 (2004) 474–482.
[40] F.-F Jin, S.-I. An, A. Timmermann, J. Zhao, Strong El Niño events and nonlinear dynamical heating, Geophys. Res. Lett. 30 (2003) 1120. doi:10.1029/2002GL016356.
[41] Y. Tang, R. Kleeman, A. Moore, A simple method for estimating variations in the predictability of ENSO, Geophy. Res. Lett. 31 (17) (2004) L17205. doi:10.1029/2004GL020673.
[42] Y. Tang, R. Kleeman, A. Moore, On the reliability of ENSO dynamical predictions, J. Atmospheric Sci. 62 (2005) 1770–1791.
[43] J.-S. Xu, H. von Storch, Predicting the state of the Southern Oscillation using principal oscillation pattern analysis, J. Clim. 3 (1990) 1316–1329.